

AeroGen: Enhancing Remote Sensing Object Detection with Diffusion-Driven Data Generation

Datao Tang¹ Xiangyong Cao^{1*} Xuan Wu¹ Jialin Li¹
 Jing Yao⁴ Xueru Bai² Dongsheng Jiang³ Yin Li³ Deyu Meng¹
¹Xi'an Jiaotong University ²Xidian University
³Huawei Technologies Ltd ⁴Chinese Academy of Sciences

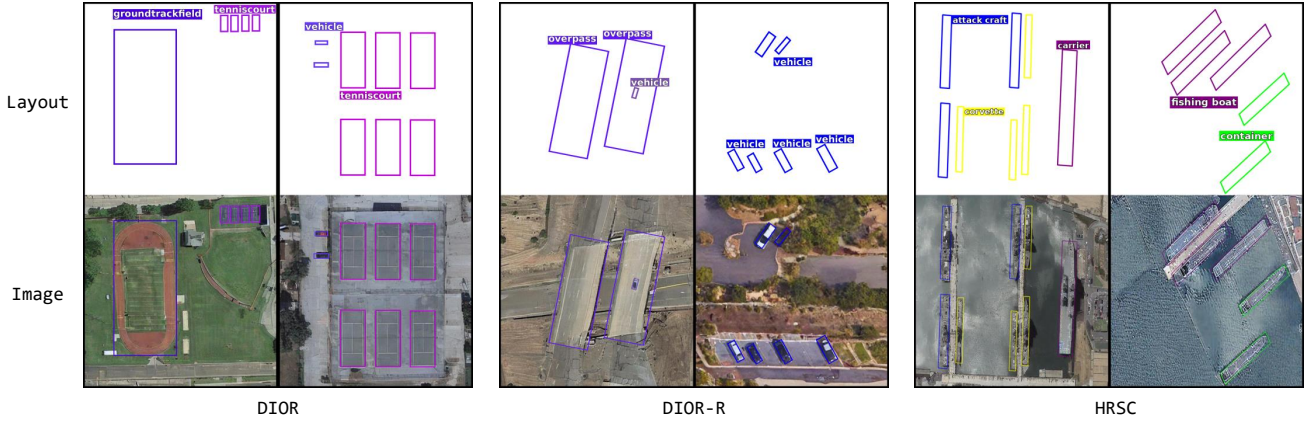


Figure 1. Generated images with our proposed AeroGen. AeroGen enables the input of both horizontal and rotated bounding box layout conditions, facilitating accurate remote sensing image layout generation.

Abstract

Remote sensing image object detection (RSIOD) aims to identify and locate specific objects within satellite or aerial imagery. However, there is a scarcity of labeled data in current RSIOD datasets, which significantly limits the performance of current detection algorithms. Although existing techniques, e.g., data augmentation and semi-supervised learning, can mitigate this scarcity issue to some extent, they are heavily dependent on high-quality labeled data and perform worse in rare object classes. To address this issue, this paper proposes a layout-controllable diffusion generative model (i.e. AeroGen) tailored for RSIOD. To our knowledge, AeroGen is the first model to simultaneously support horizontal and rotated bounding box condition generation, thus enabling the generation of high-quality synthetic images that meet specific layout and object category requirements. Additionally, we propose an end-to-end data augmentation framework that integrates a diversity-conditioned generator and a filter

ing mechanism to enhance both the diversity and quality of generated data. Experimental results demonstrate that the synthetic data produced by our method are of high quality and diversity. Furthermore, the synthetic RSIOD data can significantly improve the detection performance of existing RSIOD models, i.e., the mAP metrics on DIOR, DIOR-R, and HRSC datasets are improved by 3.7%, 4.3%, and 2.43%, respectively. The code is available at <https://github.com/Sonettoo/AeroGen>.

1. Introduction

Object detection is a key technology for understanding and analyzing remote sensing images. It enables efficient processing of large-scale satellite data to extract and identify critical information, such as land cover changes [40], urban development status [15], and the impacts of natural disasters [43]. Through object detection, researchers can automatically extract terrestrial targets from complex remote sensing images, including buildings, vehicles, roads, bridges, farmlands, and forests. This information can be further applied

*Corresponding author.

in environmental monitoring, urban planning, land use analysis, and disaster emergency management.

With the rapid development of deep learning, supervised learning-based object detection algorithms have made significant progress in remote sensing image analysis [47]. Although these algorithms can accurately locate and classify multiple objects in remote sensing images, they are heavily dependent on a large number of labelled training data. However, obtaining sufficient annotated data for remote sensing images is particularly challenging. Due to the presence of numerous and complex targets in remote sensing images, the manual annotation process is not only time-consuming and labour-intensive but also requires annotators to possess specialized knowledge, thus leading to high costs.

Although traditional data augmentation methods [3] (e.g., rotation and scaling) and enhancement techniques suitable for object detection (e.g., image mirror [14], object-centric cropping [20], and copy-paste [6]) can increase data diversity to some extent, they do not address the fundamental issue of insufficient data. The emergence of generative models [11, 24] provides a new solution to this problem. Currently, in the field of natural images, numerous high-performance generative models [26, 30] have been developed, capable of generating high-quality images from text conditions and also achieving significant progress in layout control. For remote sensing images, the application of generative models is usually combined with specific tasks, such as change detection [44], semantic segmentation [33] and road extraction [32]. These studies have been highly successful in utilizing data obtained from generative models to augment real-world datasets, thereby enhancing the performance of target models in downstream tasks. Therefore, utilizing generative diffusion models to fit the distribution of existing datasets and generate new samples to enhance the diversity and richness of remote sensing datasets is a feasible solution.

In this paper, we focus on the remote sensing image object detection (RSIOD) task and construct a layout generation model (i.e., AeroGen) specifically designed for this task. The proposed AeroGen model allows for the specification of layout prior conditions with horizontal and rotated bounding boxes, enabling the generation of high-quality remote sensing images that meet specified conditions, thus filling a gap in the research field of RSIOD. Based on the AeroGen model, we further propose a conditional generation-based end-to-end data augmentation framework. Unlike pipeline-style data augmentation schemes in the natural image domain [41], our proposed pipeline is implemented by directly synthesizing RSIOD data through conditional generative models, thus eliminating the need for additional instance-pasting procedures. By introducing a diversity-conditioned generator and generation quality evaluation, we further enhance the diversity and quality of the

generated images, thereby achieving end-to-end data augmentation for downstream object detection tasks. Moreover, we also design a novel filtering mechanism in this data augmentation pipeline to select high-quality synthetic training images, thus further boosting the performance.

In summary, the contributions of our work are threefold:

- We propose a layout-controllable diffusion model (i.e., AeroGen) specifically designed for remote sensing images. This model can generate high-quality RSIOD training datasets that conform to specified categories and spatial positions. To our knowledge, AeroGen is the first generative model to support layout conditional control for both horizontal and rotated bounding boxes.
- We design a novel end-to-end data augmentation framework that integrates the proposed AeroGen generative model with a layout condition generator as well as an image filter. This framework can produce synthetic RSIOD training datasets with high diversity and quality.
- Experimental results show that the synthetic data can improve the performance of current RSIOD models, with improvements in mAP metrics by 3.7%, 4.3%, and 2.43% on the DIOR, DIOR-R, and HRSC datasets, respectively. Notably, the performance in some rare object classes also significantly improves, e.g., achieving improvements of 17.8%, 14.7%, and 12.6% in the GF, DAM, and APO categories, respectively.

2. Related Work

2.1. Diffusion Models

Diffusion models [11, 24, 30], known for their stable training process and excellent generative capabilities, are gradually replacing Generative Adversarial Networks (GANs) [29, 39] as the dominant model in generative tasks. Text-guided diffusion models can produce realistic images, but the concise nature of text descriptions often makes it challenging to provide precise guidance for image generation, thereby limiting personalized generation capabilities. To address this issue, more researchers have introduced additional control conditions beyond text guidance, significantly expanding the application scope of diffusion models. These applications include layout guidance [16, 35, 45], style transfer [5, 36], image denoising and super-resolution [4], and video generation [12], showcasing the enormous potential of diffusion models in various complex tasks. Among these models, LDM [30] restricts the diffusion process to a low-dimensional latent space, which not only preserves the high quality of the generated images but also significantly reduces computational complexity, serving as the foundation for numerous generative studies.

2.2. Task-Oriented Data Generation

The use of generative models to synthesize training data to assist in tasks like object detection [17, 46], semantic segmentation [33] and instance segmentation [41] has garnered significant attention from researchers. Generative models not only produce artistic natural images but also quickly adapt to specific industry scenarios such as remote sensing, medical, and industrial fields through techniques like fine-tuning. For instance, A Graikos et al. [8] proposed representation-guided models that can generate embeddings rich in semantic and visual information through self-supervised learning (SSL), which guides the diffusion model to generate images. This approach reduces the difficulty of obtaining high-precision annotated data in specialized fields like histopathology and satellite imagery. In the area of remote sensing image generation, SatSynth [33] uses diffusion models to jointly learn the distribution of remote sensing images and their corresponding semantic segmentation labels. By generating semantically informed remote sensing images through joint sampling, it improves the performance of downstream segmentation tasks. Li Pang et al. [25] proposed a two-stage hyperspectral image (HSI) super-resolution framework that generates large amounts of realistic hyperspectral data for tasks like denoising and super-resolution. Moreover, models, e.g. CRS-Diff [32] and DiffusionSat [13], designed for optical remote sensing image generation, handle multiple types of conditional inputs, applying synthetic data to specific tasks such as road extraction. However, no existing research has specifically explored image generation methods for remote sensing image object detection (RSIOD) tasks. To fill this gap, we first propose a layout-controllable generative model that supports both rotated and horizontal bounding boxes, capable of synthesizing high-precision remote sensing images.

2.3. Generative Data Augmentation

To effectively apply synthetic data to downstream tasks, most existing methods directly combine synthetic data with real data for training. However, some studies (e.g., Auto Cherry-Picker [1]) have improved data quality by filtering synthetic data, thus better enhancing the performance of downstream tasks. For example, X-Paste [41] proposed a pipeline method that uses a copy-paste strategy to synthesize images, combined with a CLIP-based filtering mechanism, to further improve instance segmentation performance. A more comprehensive review of this issue can be found in DriverGen [7], which analyzes the application of synthetic data from the perspective of data distribution. It combines a copy-paste strategy to construct a multi-layer pipeline that enhances diversity and achieves significant results on the Lvis dataset [9].

The most closely related approach to our work is ODGEN [46], which employs an object-wise generation

strategy to produce consistent data for multi-object scenes, addressing the domain gap and concept bleeding issues in image generation. In contrast, our work focuses on object detection in remote sensing images, utilizing a conditional generative model to directly synthesize data, thereby avoiding the additional instance-pasting process. Furthermore, we introduce a novel diversity-conditioned generator, combined with a filtering mechanism that accounts for both diversity and generation quality, to further enhance the diversity and quality of generated images. Through this approach, we achieve end-to-end data augmentation, significantly improving the performance of downstream tasks.

3. AeroGen

In this section, we introduce AeroGen, a layout-conditional diffusion model for enhancing remote sensing image data. The model consists of two key components: (a) a remote sensing image layout generation model in Sec. 3.1 that allows users to generate high-quality RS images based on predefined layout conditions, such as horizontal and rotated boxes; (b) a generation pipeline in Sec. 3.2 that combines a diffusion-model-based diversity-conditioned generator, which produces diverse layouts aligned with physical conditions, with a data-filtering mechanism to balance the diversity and quality of synthetic data, improving the utility of the generated dataset.

3.1. Layout-conditional Diffusion Model

The model weights, obtained through comprehensive fine-tuning on a remote sensing dataset based on LDM [30, 32], are adopted for RS study. In the original text-to-image diffusion model, the conditional position information is combined with the text control condition, and layout-based remote sensing image generation is achieved by establishing a unified position information encoding along with a corresponding dual cross-attention network, as shown in Fig. 2. Building on the latest research advances, combined with the regional layout mask-attention strategy, control accuracy is improved, particularly for small target regions.

Layout Embedding. As shown in Fig. 2(a), each object’s bounding box or rotational bounding box is uniformly represented as a list of eight coordinates, i.e., $\mathbf{x} = [x_1, y_1, \dots, x_4, y_4]$, ensuring a consistent representation between horizontal and rotated bounding boxes. Building on this, Fourier [23] encoding is employed to convert these positional coordinates into a frequency domain vector representation, similar to GLIGEN [16]. We use a frozen CLIP text encoder [27] to obtain fixed codes \mathbf{c} for different categories, which serve as layout condition inputs. The Fourier-encoded coordinates are then fused with the category encodings using an additional linear layer to produce the lay-

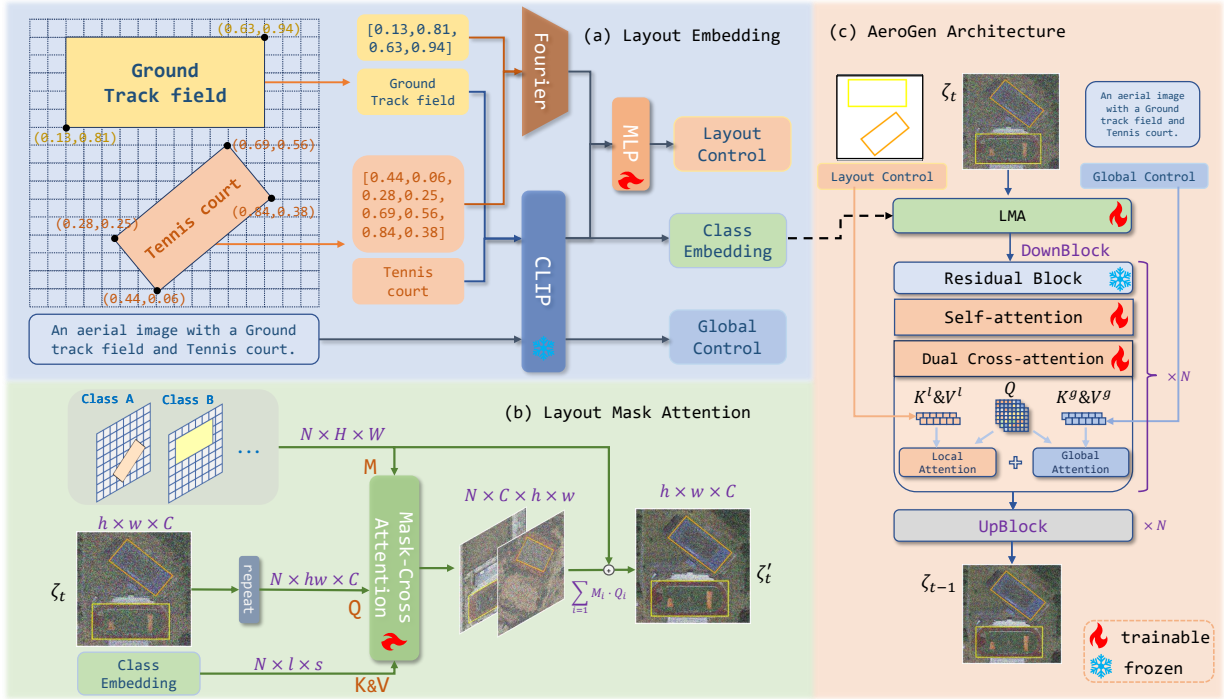


Figure 2. AeroGen’s overall architecture. (a) The layout embedding module combines bounding box coordinates with vectorized semantic information using Fourier and MLP layers. This encodes layout information to facilitate control, with the prompt description processed by a CLIP text encoder for global conditional guidance. (b) The injection of layout information at the noise level is demonstrated, where a local mask governs the injection position of the layout information, allowing for finer layout control. (c) The overall architecture and training process of AeroGen. At each timestep, the image being denoised first passes through a layout information injection module, which enhances layout conditional guidance.

out control input:

$$\mathbf{h} = \text{Linear}([\gamma(\mathbf{x}); \mathbf{c}]), \quad (1)$$

where $[\gamma(\mathbf{x}); \mathbf{c}]$ denotes the concatenation of Fourier-coded coordinates and category codes, and $\text{Linear}(\cdot)$ represents the linear transformation layer. In this manner, spatial location and category information are effectively combined as layout control tokens.

Layout Mask Attention. In addition to traditional token-based control, recent studies indicate that direct semantic embedding based on feature maps is also an effective method for layout guidance. In the denoising process of a diffusion model, the injection of conditional information is gradual, enabling local attribute editing at the noise level. To this end, conditionally encoded noise region steering is employed and combined with a cropping step for improved layout precision. As shown in Fig. 2(b), each bounding box is first transformed into a 0/1 mask M , and category attributes are obtained through CLIP encoding. During each denoising step, the mask attention network provides additional layout guidance. The process is expressed as follows: for each denoised image Q and category encoding K, V , the

mask M is used for attention computation according to the following equation:

$$\mathcal{Q} = \sum_{i=1}^n M_i \cdot \text{softmax} \left(\frac{Q K_i^\top}{\sqrt{d_k}} + \mathcal{M}_i \right) V_i,$$

where M represents the corresponding bounding box mask, and \mathcal{M}_i derived from M_i as the attention mask. This method enables precise manipulation of local noise characteristics during the diffusion generation process, offering finer control over the image layout.

AeroGen Architecture. In AeroGen, the text prompt serves as a global condition and is integrated with layout control tokens via a dual cross-attention mechanism. The output is computed as:

$$\text{Out} = \Psi(Q, K^g, V^g) + \lambda \cdot \Psi(Q, K^l, V^l), \quad (2)$$

where Ψ represents the cross-attention mechanism. K^g and V^g are the keys and values of the global text condition, while K^l and V^l are the layout control tokens. λ balances the influence of global and layout conditions.

The overall loss function for AeroGen combines both the

global text condition and layout control, defined as:

$$\mathcal{L} = \mathbb{E} \left[\|\epsilon - \epsilon_\theta(\mathbf{x}_t, t, \mathbf{c}^g, \mathbf{c}^l)\|^2 \right], \quad (3)$$

where \mathbf{x}_t represents the noisy image at time step t , \mathbf{c}^g is the global text condition, and \mathbf{c}^l is the layout control.

3.2. Generative Pipeline

The layout generative pipeline, as illustrated in Fig. 3, is divided into five stages: label generation, label filter, image generation, image filter, and data augmentation. Each generation step is followed by a corresponding screening step to ensure synthesis quality.

Label Generation. Inspired by recent cutting-edge research [33], we adopt a denoising diffusion probabilistic model (DDPM [11]) to learn the conditional distribution and directly sample from it to obtain layout labels, thereby avoiding conflicts in layout conditions that may arise from random synthesis approaches. The specific method is illustrated in Fig. 3, where a labelling matrix \mathbf{M}_L is first constructed. This matrix contains all categories of conditions with dimensions $H \times W \times N$, where H and W represent the height and width of the images, respectively, and N denotes the number of condition categories. For each condition corresponding to the target frame of the image, the value within the target frame region is set to 1, while the values in the remaining regions are set to -1. This process is formally represented as:

$$\mathbf{M}_L(i, j, k) = \begin{cases} 1, & \text{if } (i, j) \in \mathcal{R}_k, \\ -1, & \text{if } (i, j) \notin \mathcal{R}_k, \end{cases} \quad (4)$$

where $i \in \{1, \dots, H\}$, $j \in \{1, \dots, W\}$, and $k \in \{1, \dots, N\}$, with \mathcal{R}_k denoting the target area for the k -th category. Next, this conditional distribution is fitted using a DDPM-based generator G_θ . The loss function is based on the mean square error (MSE):

$$\mathcal{L} = \mathbb{E} \left[\|\epsilon - \epsilon_\theta(\mathbf{M}_L^{(t)}, t)\|^2 \right], \quad (5)$$

where $\mathbf{M}_L^{(0)}$ represents the original layout matrix, $\mathbf{M}_L^{(t)}$ represents the noise matrix at the t -th time step, and $\epsilon_\theta(\mathbf{M}_L^{(t)}, t)$ denotes the model's predicted noise at step t .

Label Filter and Enhancement. The label data sampled from the generator may not always align with real-world intuition or effectively guide image generation. Therefore, we propose a normal distribution-based filtering mechanism to screen the generated bounding box information, ensuring that the data conform to the distribution characteristics of real labels. The label filter assumes that the attributes of the bounding boxes (e.g., area) follow a normal distribution ($\mathcal{N}(\mu_X, \sigma_X^2)$) and introduces the following constraint:

Dataset	Modality	Images	Objects	Categories
DIOR [15]	HBB	23,463	192,518	20
DIOR-R [2]	OBB	23,463	192,518	20
HRSC [21]	OBB	1,061	2,976	19

Table 1. Statistical information of the benchmark RSIOD datasets.

$\frac{(X - \mu_X)}{\sigma_X} \leq \epsilon$, where ϵ determines the filter's strictness, thereby ensuring that generated bounding boxes fall within a realistic and feasible range. Synthetic pseudo-labels and genuine a priori labels are filtered to form a comprehensive layout condition pool through additional enhancement strategies, including scaling, panning, rotating, and flipping.

Image Generation. The synthetic bounding box labels are obtained based on the pool of layout conditions. The corresponding synthetic images are generated using the layout-guided diffusion model through the image generation process described in Sec. 3.1. The model uses these bounding box labels to guide the generation, ensuring that the image content matches the generated layout conditions.

Image Filter. Since the images generated by the diffusion model do not consistently meet high-quality or predefined layout requirements, a screening mechanism is implemented to evaluate both the quality of the generation and the consistency of the layout. The consistency of the semantic and layout is evaluated using the CLIP model [19] and a ResNet101-based classifier [10]. Synthetic images are then filtered by calculating their CLIP scores and minimum classification accuracies, which are compared against predefined thresholds to select the final filtered images.

Data Augmentation. The synthetic data serves as a complementary dataset alongside the real dataset, and both are utilized as training data for downstream target detection model training.

4. Experiments

In this section, we conducted extensive experiments to verify the generative capabilities of AeroGen and its auxiliary data augmentation ability to support downstream RSIOD tasks. Specifically, we assessed the performance of our layout generation model AeroGen from both quantitative and qualitative perspectives. Subsequently, we performed data augmentation experiments on three datasets (i.e., DIOR, DIOR-R, and HRSC) to verify the effectiveness of synthetic data generated by our AeroGen model in improving the performance of downstream object detection tasks.

4.1. Implementation Details

Data Preparation. An overview of the three datasets is provided in Tab. 1. Notably, the DIOR and DIOR-R datasets [2] share the same image data but differ in annotation format, with DIOR using bounding boxes and DIOR-R using

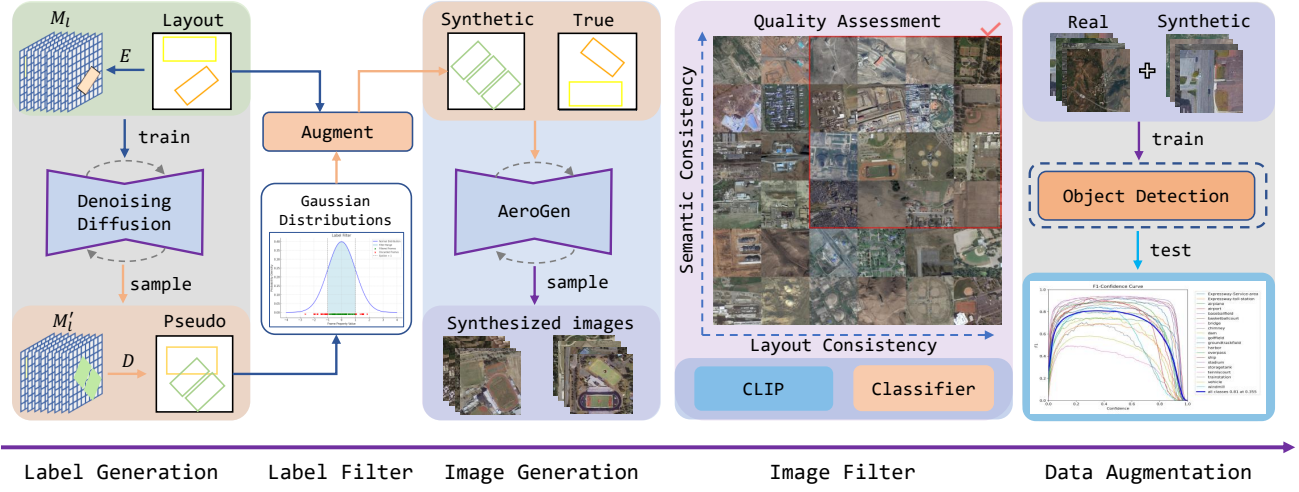


Figure 3. Overview of the pipeline based on AeroGen. By fitting the conditional distribution using a diffusion model, we expand a diverse set of layout conditions and combine them with AeroGen to generate synthetic data. Additionally, we introduce two filters to eliminate low-quality synthetic conditions and images, further ensuring the semantic consistency and layout consistency of the synthetic images. Finally, we incorporate synthetic images alongside real images in the training set to improve the performance of downstream tasks.

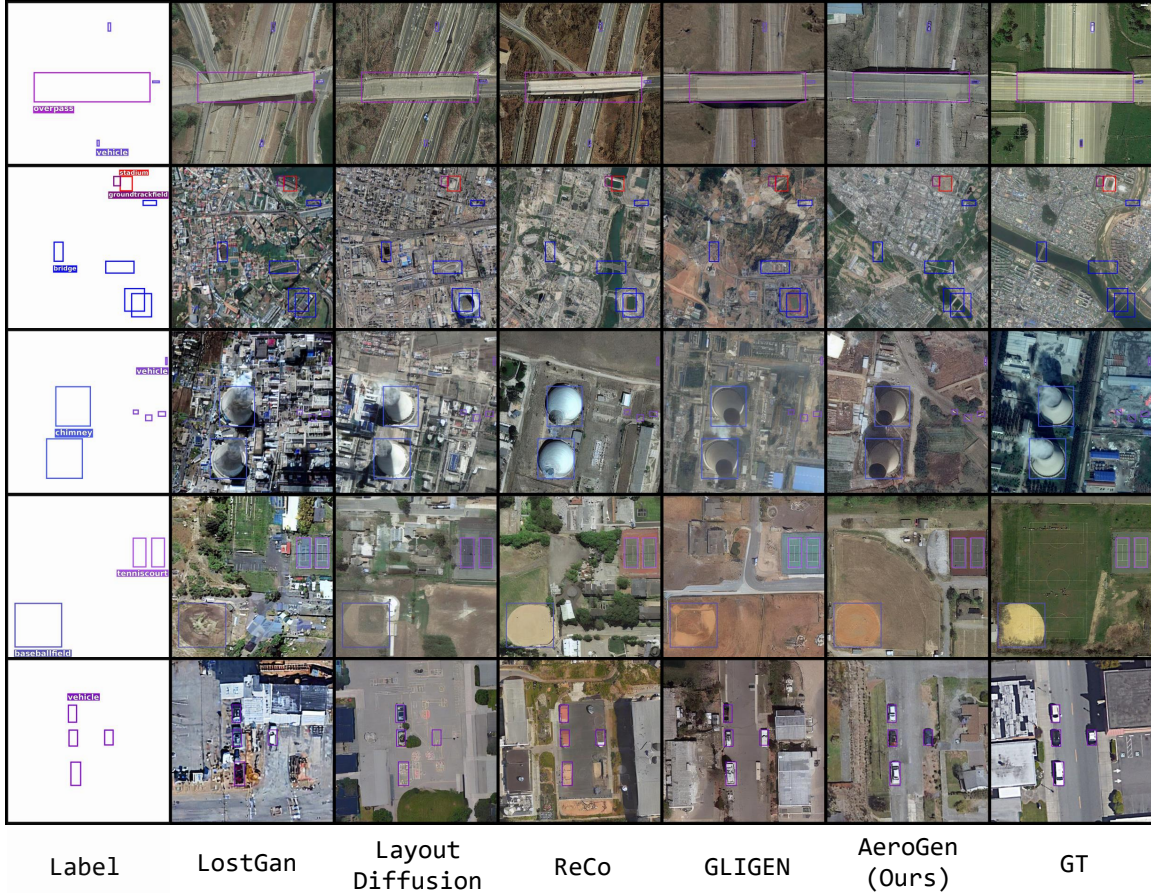


Figure 4. Visualization comparison of the generated image by different methods on the DIOR dataset.

rotated bounding boxes. HRSC [21] is a Remote Sensing dataset for ship detection, with image sizes ranging from 300×300 to 1500×900 pixels. It is divided into 436, 181, and 444 frames for training, evaluation, and testing, respectively. The DIOR/DIOR-R dataset is split into training, validation, and testing sets in a 1:1:2 ratio, with generative model training conducted exclusively on the training set.

Training Details. We trained our AeroGen separately on each dataset for 100 epochs. During training, we used the AdamW optimizer [22] with a learning rate of 1e-5. Only the attention layers of UNet and the Layout Mask Attention (LMA) are updated, while the remaining weights are inherited from the fine-tuned LDM in RS data [32].

Evaluation Metrics. For the quantitative analysis of generated images, we used the FID score to evaluate the visual quality of the generated images and employed Classification Score (CAS) [28] and YOLO Score [18] to measure the layout consistency of the generated images. In the data augmentation experiments, we assessed object detection model performance based on mAP50 and mAP50-95 (mAP) metrics to evaluate their overall quality.

4.2. Image Quality Results

Quantitative Evaluation. We used a bounding box condition defined by four extreme coordinates and conducted both training and testing on the DIOR dataset. We compared AeroGen with state-of-the-art layout-to-image generation methods, including LostGAN [31], ReCo [38], LayoutDiffusion[42], and GLIGEN [16]. The performance of these methods on three metrics is reported in Tab. 2. To ensure fairness, we initialized all methods with identical SD weights and trained them on the DIOR dataset for the same number of epochs. Our method outperformed other methods across all the metrics.

Furthermore, we evaluated AeroGen and GLIGEN on the DIOR-R and HRSC datasets with rotated bounding boxes, where AeroGen consistently excelled. Notably, the original GliGen method does not support rotated bounding box conditions; therefore, we modified the layout encoding (as shown in Fig. 2 (a)) and retrained the model.

Qualitative Evaluation. Fig. 4 compares the results of AeroGen with those of other methods. AeroGen shows superior layout consistency and an enhanced capability for generating small objects. Besides, we present experimental results on natural images in the supplemental material.

4.3. Data Augmentation Experiments

We synthesize data on three RSIOD datasets for data augmentation. For the DIOR/DIOR-R datasets, we synthesized 10k, 20k, and 50k samples for the RSIOD task. For the HRSC dataset, we synthesize 2k, 4k, and 10k data in the same ratio. The training was performed using the OBB branch experimental setup of the unified YOLOv8 [34] and

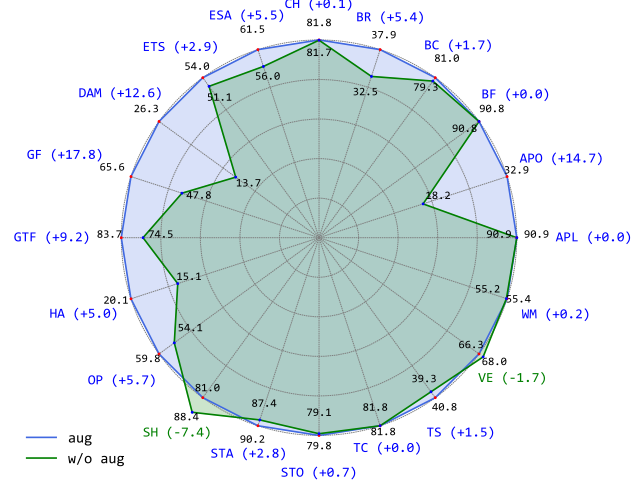


Figure 5. Comparison of mAP50 across each category on the DIOR-R dataset under the setting of data augmentation with 50k generation images (aug) and without augmentation (w/o aug).

Oriented R-CNN [37] RSIOD models, and the model performance is verified on the corresponding test sets. The experimental results are shown in Tab. 3. The addition of synthetic data significantly improves performance on downstream tasks

We visualize the mAP scores for different categories in detail, as shown in Fig. 5. In most categories, results incorporating enhancements significantly outperform those without them, particularly in rarer categories, achieving improvements of 17.8%, 14.7%, and 12.6% in the GF, DAM, and APO categories, respectively.

4.4. Ablation Study

Ablation of Enhanced Methods. We compared synthetic data enhancement methods with traditional approaches, including the basic enhancement techniques of Flip and Copy-Paste [6] for target detection tasks, as shown in Tab. 4. The target detection model trained on synthetic data performs significantly better than when trained with traditional methods, demonstrating the generative model’s effectiveness for data enhancement.

Ablation of Different Modules. We assessed the impact of different modules on image quality generated by AeroGen in Tab. 5. The contribution of each module to the enhancement of image quality is evaluated by incorporating additional components into the original SD model. Results show that Layout Mask Attention (LMA) effectively captures global semantic information and preserves layout consistency, while adding Dual Cross Attention (DCA) further enhances performance, particularly in YOLO Score, indicating improved regional target generation. Overall, the model performs best when both LMA and DCA are used.

Method	Dataset	Modality	FID ↓	CAS ↑	YOLO Score ↑
LostGAN [31]	DIOR [15]	HBB	57.10	46.02	14.3/27.3/15.2
Layout Diffusion [42]			45.31	56.98	20.0/37.4/19.3
ReCo [38]			42.56	55.42	21.1/40.7/23.1
GLIGEN [16]			41.31	63.50	25.8/44.4/27.8
AeroGen (Ours)			38.57	76.84	29.8/54.2/31.6
GLIGEN [16]†	DIOR-R [2]	OBB	48.43	58.89	24.6/41.6/25.1
AeroGen (Ours)			35.07	74.13	29.6/57.6/32.0
GLIGEN [16]†	HRSC [21]	OBB	66.69	43.35	23.4/44.7/26.3
AeroGen (Ours)			45.86	51.19	27.1/51.0/27.6

Table 2. Quantitative results of the generated images by different methods. For the Oriented Bounding Box (OBB) modality, we replicated the GLIGEN† method to account for the rotated bounding box. The best results are in **bold**.

Gen Data	mAP ↑	mAP50 ↑	Gen Data	mAP ↑	mAP50 ↑	Gen Data	mAP ↑	mAP50 ↑
0	54.22	72.69	0	37.39	60.21	0	63.49	90.28
10k	55.62	74.79	10k	39.81	62.39	2k	64.12	91.79
20k	56.78	76.31	20k	41.12	63.33	4k	64.78	92.31
50k	57.92	77.10	50k	41.69	64.12	10k	65.92	93.10

(a) DIOR

(b) DIOR-R

(c) HRSC

Table 3. The enhancement effects of various scales of synthetic data on downstream tasks across DIOR, DIOR-R, and HRSC datasets.

Strategy	mAP ↑	mAP50 ↑
Flip	37.39	60.21
CopyPaste [6]	38.25	61.79
AeroGen	41.32	63.98
CopyPaste + Flip [6]	38.75	62.11
AeroGen + Flip	41.69	64.12

Table 4. Comparison of different augmentation strategies on the DIOR-R dataset.

LMA	DCA	FID ↓	CAS ↑	YOLO Score ↑
✗	✗	82.11	18.48	1.3/3.9/1.1
✗	✓	66.29	40.71	16.5/29.2/17.7
✓	✗	61.50	50.11	25.3/46.5/27.2
✓	✓	38.57	76.84	29.8/54.2/31.6

Table 5. Ablation study of different modules in the AeroGen model on the DIOR dataset.

Ablation of Augment Pipeline. We further analyze the filtering strategies and data augmentation techniques in the generation pipeline, including diverse generation strategies, filtering strategies for layout conditions, and filtering strategies for layout and semantic consistency of images. We use the synthetic data generated in various ways as enhancement data and conduct enhancement experiments on the DIOR-R datasets and the experimental results are shown in

Synthesis	Layout Diversity		Image Quality		Metrics	
	Filter	Augment	Semantic	Layout	mAP ↑	mAP50 ↑
✓	✓	✓	✓	✓	41.69	64.12
✗	✗	✓	✓	✓	41.31	63.47
✓	✗	✓	✓	✓	40.92	62.41
✓	✓	✗	✓	✓	39.62	61.32
✓	✓	✓	✗	✓	40.27	62.13
✓	✓	✓	✓	✗	37.05	60.03

Table 6. Ablation study results analyzing the impact of diverse generation and filtering strategies in the synthesis pipeline on layout labeling and image filtering consistency.

Tab. 6. As can be seen, each component in the generation pipeline contributes positively.

5. Conclusion

This paper introduces AeroGen, a layout-controllable diffusion model designed to enhance remote sensing image datasets for target detection. The model comprises two primary components: a layout generation model that creates high-quality remote sensing images based on predefined layout conditions, and a data generation pipeline that incorporates a diversity of condition generators for the diffusion model. The pipeline employs a double filtering mechanism to exclude low-quality generation conditions and images,

thereby ensuring the semantic and layout consistency of the generated images. By combining synthetic and real images in the training set, AeroGen significantly improves model performance in downstream tasks. This work highlights the potential of generative modeling in enhancing the datasets of remote sensing image processing tasks.

References

- [1] Yicheng Chen, Xiangtai Li, Yining Li, Yanhong Zeng, Jianzong Wu, Xiangyu Zhao, and Kai Chen. Auto cherry-picker: Learning from high-quality generative data driven by language. *arXiv preprint arXiv:2406.20085*, 2024. [3](#)
- [2] Gong Cheng, Jiabao Wang, Ke Li, Xingxing Xie, Chunbo Lang, Yanqing Yao, and Junwei Han. Anchor-free oriented proposal generator for object detection. *IEEE Transactions on Geoscience and Remote Sensing*, 60:1–11, 2022. [5, 8](#)
- [3] Phillip Chlap, Hang Min, Nym Vandenberg, Jason Dowling, Lois Holloway, and Annette Haworth. A review of medical image data augmentation techniques for deep learning applications. *Journal of Medical Imaging and Radiation Oncology*, 65(5):545–563, 2021. [2](#)
- [4] Hyungjin Chung, Eun Sun Lee, and Jong Chul Ye. Mr image denoising and super-resolution using regularized reverse diffusion. *IEEE Transactions on Medical Imaging*, 42(4): 922–934, 2022. [2](#)
- [5] Jiwoo Chung, Sangeek Hyun, and Jae-Pil Heo. Style injection in diffusion: A training-free approach for adapting large-scale diffusion models for style transfer. In *Proceedings of the IEEE/CVF Conference on Computer Vision and Pattern Recognition*, pages 8795–8805, 2024. [2](#)
- [6] Debidatta Dwibedi, Ishan Misra, and Martial Hebert. Cut, paste and learn: Surprisingly easy synthesis for instance detection. In *Proceedings of the IEEE international conference on computer vision*, pages 1301–1310, 2017. [2, 7, 8](#)
- [7] Chengxiang Fan, Muzhi Zhu, Hao Chen, Yang Liu, Weijia Wu, Huaqi Zhang, and Chunhua Shen. Divergen: Improving instance segmentation by learning wider data distribution with more diverse generative data. In *Proceedings of the IEEE/CVF Conference on Computer Vision and Pattern Recognition*, pages 3986–3995, 2024. [3](#)
- [8] Alexandros Graikos, Srikar Yellapragada, Minh-Quan Le, Saarthak Kapse, Prateek Prasanna, Joel Saltz, and Dimitris Samaras. Learned representation-guided diffusion models for large-image generation. In *Proceedings of the IEEE/CVF Conference on Computer Vision and Pattern Recognition*, pages 8532–8542, 2024. [3](#)
- [9] Agrim Gupta, Piotr Dollar, and Ross Girshick. Lvis: A dataset for large vocabulary instance segmentation. In *Proceedings of the IEEE/CVF conference on computer vision and pattern recognition*, pages 5356–5364, 2019. [3](#)
- [10] Kaiming He, Xiangyu Zhang, Shaoqing Ren, and Jian Sun. Deep residual learning for image recognition. In *Proceedings of the IEEE conference on computer vision and pattern recognition*, pages 770–778, 2016. [5](#)
- [11] Jonathan Ho, Ajay Jain, and Pieter Abbeel. Denoising diffusion probabilistic models. *Advances in neural information processing systems*, 33:6840–6851, 2020. [2, 5](#)
- [12] Jonathan Ho, William Chan, Chitwan Saharia, Jay Whang, Ruiqi Gao, Alexey Gritsenko, Diederik P Kingma, Ben Poole, Mohammad Norouzi, David J Fleet, et al. Imagen video: High definition video generation with diffusion models. *arXiv preprint arXiv:2210.02303*, 2022. [2](#)
- [13] Samar Khanna, Patrick Liu, Linqi Zhou, Chenlin Meng, Robin Rombach, Marshall Burke, David B Lobell, and Stefano Ermon. Diffusionsat: A generative foundation model for satellite imagery. In *The Twelfth International Conference on Learning Representations*, 2023. [3](#)
- [14] Mate Kisantal. Augmentation for small object detection. *arXiv preprint arXiv:1902.07296*, 2019. [2](#)
- [15] Ke Li, Gang Wan, Gong Cheng, Liqiu Meng, and Junwei Han. Object detection in optical remote sensing images: A survey and a new benchmark. *ISPRS journal of photogrammetry and remote sensing*, 159:296–307, 2020. [1, 5, 8](#)
- [16] Yuheng Li, Haotian Liu, Qingyang Wu, Fangzhou Mu, Jianwei Yang, Jianfeng Gao, Chunyuan Li, and Yong Jae Lee. Gligen: Open-set grounded text-to-image generation. In *Proceedings of the IEEE/CVF Conference on Computer Vision and Pattern Recognition*, pages 22511–22521, 2023. [2, 3, 7, 8](#)
- [17] Yuhang Li, Xin Dong, Chen Chen, Weiming Zhuang, and Lingjuan Lyu. A simple background augmentation method for object detection with diffusion model. *arXiv preprint arXiv:2408.00350*, 2024. [3](#)
- [18] Zejian Li, Jingyu Wu, Immanuel Koh, Yongchuan Tang, and Lingyun Sun. Image synthesis from layout with locality-aware mask adaption. In *Proceedings of the IEEE/CVF International Conference on Computer Vision*, pages 13819–13828, 2021. [7](#)
- [19] Fan Liu, Delong Chen, Zhangqinyun Guan, Xiaocong Zhou, Jiale Zhu, Qiaolin Ye, Liyong Fu, and Jun Zhou. Remoteclip: A vision language foundation model for remote sensing. *IEEE Transactions on Geoscience and Remote Sensing*, 2024. [5](#)
- [20] Wei Liu, Dragomir Anguelov, Dumitru Erhan, Christian Szegedy, Scott Reed, Cheng-Yang Fu, and Alexander C Berg. Ssd: Single shot multibox detector. In *Computer Vision–ECCV 2016: 14th European Conference, Amsterdam, The Netherlands, October 11–14, 2016, Proceedings, Part I* 14, pages 21–37. Springer, 2016. [2](#)
- [21] Zikun Liu, Hongzhen Wang, Lubin Weng, and Yiping Yang. Ship rotated bounding box space for ship extraction from high-resolution optical satellite images with complex backgrounds. *IEEE geoscience and remote sensing letters*, 13(8): 1074–1078, 2016. [5, 7, 8](#)
- [22] I Loshchilov. Decoupled weight decay regularization. *arXiv preprint arXiv:1711.05101*, 2017. [7](#)
- [23] Ben Mildenhall, Pratul P Srinivasan, Matthew Tancik, Jonathan T Barron, Ravi Ramamoorthi, and Ren Ng. Nerf: Representing scenes as neural radiance fields for view synthesis. *Communications of the ACM*, 65(1):99–106, 2021. [3](#)
- [24] Alexander Quinn Nichol and Prafulla Dhariwal. Improved denoising diffusion probabilistic models. In *International conference on machine learning*, pages 8162–8171. PMLR, 2021. [2](#)

[25] Li Pang, Datao Tang, Shuang Xu, Deyu Meng, and Xiangyong Cao. Hsigene: A foundation model for hyperspectral image generation. *arXiv preprint arXiv:2409.12470*, 2024. 3

[26] Dustin Podell, Zion English, Kyle Lacey, Andreas Blattmann, Tim Dockhorn, Jonas Müller, Joe Penna, and Robin Rombach. Sdxl: Improving latent diffusion models for high-resolution image synthesis. *arXiv preprint arXiv:2307.01952*, 2023. 2

[27] Alec Radford, Jong Wook Kim, Chris Hallacy, Aditya Ramesh, Gabriel Goh, Sandhini Agarwal, Girish Sastry, Amanda Askell, Pamela Mishkin, Jack Clark, et al. Learning transferable visual models from natural language supervision. In *International Conference on Machine Learning*, pages 8748–8763. PMLR, 2021. 3

[28] Suman Ravuri and Oriol Vinyals. Classification accuracy score for conditional generative models. *Advances in neural information processing systems*, 32, 2019. 7

[29] Scott Reed, Zeynep Akata, Xinchen Yan, Lajanugen Logeswaran, Bernt Schiele, and Honglak Lee. Generative adversarial text to image synthesis. In *International conference on machine learning*, pages 1060–1069. PMLR, 2016. 2

[30] Robin Rombach, Andreas Blattmann, Dominik Lorenz, Patrick Esser, and Björn Ommer. High-resolution image synthesis with latent diffusion models. In *Proceedings of the IEEE/CVF conference on computer vision and pattern recognition*, pages 10684–10695, 2022. 2, 3

[31] Wei Sun and Tianfu Wu. Image synthesis from reconfigurable layout and style. In *Proceedings of the IEEE/CVF International Conference on Computer Vision*, pages 10531–10540, 2019. 7, 8

[32] Datao Tang, Xiangyong Cao, Xingsong Hou, Zhongyuan Jiang, Junmin Liu, and Deyu Meng. Crs-diff: Controllable remote sensing image generation with diffusion model. *IEEE Transactions on Geoscience and Remote Sensing*, 2024. 2, 3, 7

[33] Aysim Toker, Marvin Eisenberger, Daniel Cremers, and Laura Leal-Taixé. Satsynth: Augmenting image-mask pairs through diffusion models for aerial semantic segmentation. In *Proceedings of the IEEE/CVF Conference on Computer Vision and Pattern Recognition*, pages 27695–27705, 2024. 2, 3, 5

[34] Rejin Varghese and M Sambath. Yolov8: A novel object detection algorithm with enhanced performance and robustness. In *2024 International Conference on Advances in Data Engineering and Intelligent Computing Systems (ADICS)*, pages 1–6. IEEE, 2024. 7

[35] Xudong Wang, Trevor Darrell, Sai Saketh Rambhatla, Rohit Girdhar, and Ishan Misra. Instancediffusion: Instance-level control for image generation. In *Proceedings of the IEEE/CVF Conference on Computer Vision and Pattern Recognition*, pages 6232–6242, 2024. 2

[36] Zhizhong Wang, Lei Zhao, and Wei Xing. Stylediffusion: Controllable disentangled style transfer via diffusion models. In *Proceedings of the IEEE/CVF International Conference on Computer Vision*, pages 7677–7689, 2023. 2

[37] Xingxing Xie, Gong Cheng, Jiabao Wang, Xiwen Yao, and Junwei Han. Oriented r-cnn for object detection. In *Proceedings of the IEEE/CVF international conference on computer vision*, pages 3520–3529, 2021. 7

[38] Zhengyuan Yang, Jianfeng Wang, Zhe Gan, Linjie Li, Kevin Lin, Chenfei Wu, Nan Duan, Zicheng Liu, Ce Liu, Michael Zeng, et al. Reco: Region-controlled text-to-image generation. In *Proceedings of the IEEE/CVF Conference on Computer Vision and Pattern Recognition*, pages 14246–14255, 2023. 7, 8

[39] Han Zhang, Tao Xu, Hongsheng Li, Shaoting Zhang, Xiaogang Wang, Xiaolei Huang, and Dimitris N Metaxas. Stackgan: Text to photo-realistic image synthesis with stacked generative adversarial networks. In *Proceedings of the IEEE international conference on computer vision*, pages 5907–5915, 2017. 2

[40] Xin Zhang, Liangxiu Han, Lianghao Han, and Liang Zhu. How well do deep learning-based methods for land cover classification and object detection perform on high resolution remote sensing imagery? *Remote Sensing*, 12(3):417, 2020. 1

[41] Hanqing Zhao, Dianmo Sheng, Jianmin Bao, Dongdong Chen, Dong Chen, Fang Wen, Lu Yuan, Ce Liu, Wenbo Zhou, Qi Chu, et al. X-paste: Revisiting scalable copy-paste for instance segmentation using clip and stablediffusion. In *International Conference on Machine Learning*, pages 42098–42109. PMLR, 2023. 2, 3

[42] Guangcong Zheng, Xianpan Zhou, Xuewei Li, Zhongang Qi, Ying Shan, and Xi Li. Layoutdiffusion: Controllable diffusion model for layout-to-image generation. In *Proceedings of the IEEE/CVF Conference on Computer Vision and Pattern Recognition*, pages 22490–22499, 2023. 7, 8

[43] Zhuo Zheng, Yanfei Zhong, Junjue Wang, Ailong Ma, and Liangpei Zhang. Building damage assessment for rapid disaster response with a deep object-based semantic change detection framework: From natural disasters to man-made disasters. *Remote Sensing of Environment*, 265:112636, 2021. 1

[44] Zhuo Zheng, Stefano Ermon, Dongjun Kim, Liangpei Zhang, and Yanfei Zhong. Changen2: Multi-temporal remote sensing generative change foundation model. *IEEE Transactions on Pattern Analysis and Machine Intelligence*, 2024. 2

[45] Deweui Zhou, You Li, Fan Ma, Xiaoting Zhang, and Yi Yang. Migc: Multi-instance generation controller for text-to-image synthesis. In *Proceedings of the IEEE/CVF Conference on Computer Vision and Pattern Recognition*, pages 6818–6828, 2024. 2

[46] Jingyuan Zhu, Shiyu Li, Yuxuan Liu, Ping Huang, Jiulong Shan, Huimin Ma, and Jian Yuan. Odgen: Domain-specific object detection data generation with diffusion models. *arXiv preprint arXiv:2405.15199*, 2024. 3

[47] Zhengxia Zou, Keyan Chen, Zhenwei Shi, Yuhong Guo, and Jieping Ye. Object detection in 20 years: A survey. *Proceedings of the IEEE*, 111(3):257–276, 2023. 2

AeroGen: Enhancing Remote Sensing Object Detection with Diffusion-Driven Data Generation

Supplementary Material

6. Limitations

Despite AeroGen’s notable advancements in generating tiny objects and enhancing datasets, some limitations persist. Firstly, the quality of AeroGen-generated data decreases markedly as the number of instances grows, especially beyond 20 objects, highlighting the need for enhanced performance in complex scenarios. Additionally, AeroGen supports only fixed-category generation in closed environments, restricting flexibility and limiting its applicability to diverse open-domain requirements, particularly for fine-grained control, which necessitates further refinement. While CLIP has been integrated to reduce instance confusion, it shows limited capability in understanding tiny targets in remote sensing images, potentially undermining generation accuracy. Moreover, the final augmented dataset is directly merged with real data for training. However, optimizing this process and developing more effective training strategies remain critical challenges.

7. AeroGen Implementation Details

We utilized three datasets, including DIOR/DIOR-R, with a 1:1:2 division for the training, validation, and test sets. Each category is accompanied by tailored text descriptions and a uniform prompt template applied to the entire image, as shown in Tab. 7. In the HRSC dataset, the most detailed categories were employed at each stage of generation, with all 19 categories encoded within the training set.

Training, testing, and data augmentation were performed on all three datasets, with images consistently resized to 512×512 dimensions using cropping, resizing, and other preprocessing techniques. Experiments employed the original SD 1.5 weights, training the DIOR/DIOR-R dataset for 100 epochs and HRSC for 20 epochs using the AdamW optimizer with a learning rate of 1e-5. All experiments were performed on an NVIDIA GeForce RTX 4090 GPU with a batch size of 4. In experiments with the Layout Mask Attention module, layout information was incorporated during the initial diffusion phase (timesteps 0–500) and transitioned to the text-to-image generation stage (timesteps 500–1000) to ensure the quality of synthetic data, as shown in Fig. 6.

ID	Abbreviation	Category	Description
0	APL	airplane	airplane parked on the ground
1	APO	airport	busy airport
2	BF	baseballfield	green baseball field
3	BC	basketballcourt	outdoor basketball court
4	BR	bridge	long bridge
5	CH	chimney	tall chimney
6	DAM	dam	large dam
7	ESA	Expressway-Service-area	crowded expressway service area
8	ETS	Expressway-toll-station	busy expressway toll station
9	GF	golffield	well-maintained golf field
10	GTF	groundtrackfield	athletic ground track field
11	HA	harbor	bustling harbor
12	OP	overpass	elevated overpass
13	SH	ship	ship on the water
14	STA	stadium	large stadium
15	STO	storagetank	industrial storage tank
16	TC	tenniscourt	clay tennis court
17	TS	trainstation	crowded train station
18	VE	vehicle	vehicle on the road
19	WM	windmill	rotating windmill

Table 7. Category, abbreviation, and description Correspondence of the DIOR/DIOR-R dataset.

No.	Category ID	Category Name
0	100000001	aircraft_carrier
1	100000003	amphibious_assault_ship
2	100000004	submarine
3	100000005	destroyer
4	100000006	frigate
5	100000007	corvette
6	100000008	patrol_vessel
7	100000009	landing_ship
8	100000010	mine_sweeper
9	100000011	fast_attack_craft
10	100000012	supply_ship
11	100000013	medical_ship
12	100000015	research_vessel
13	100000016	fishing_boat
14	100000017	cruise_ship
15	100000018	cargo_ship
16	100000019	container_ship
17	100000020	tugboat
18	100000022	oil_tanker

Table 8. Category ID to name mapping of the HRSC dataset.

8. AeroGen Additional Implementation Details

8.1. Qualitative results

In this section, we complement the results with more visualisations on the three datasets, as shown in Fig. 8. In addition, we provided additional analyses of AeroGen’s diversity to further demonstrate its generative capabilities, as illustrated in Fig.

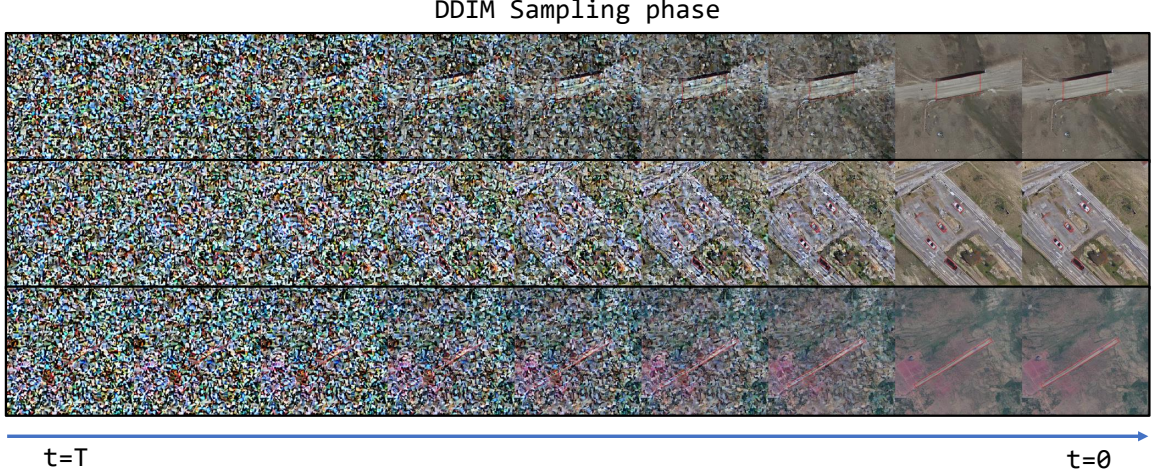


Figure 6. Visualisation of the AeroGen generation process.

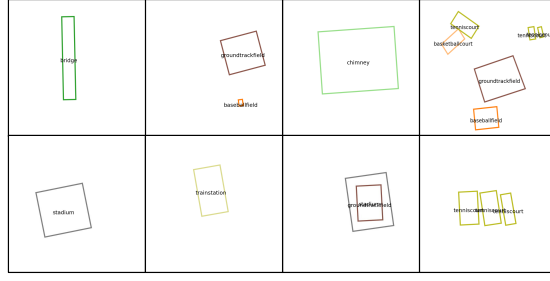


Figure 7. Synthesis of layout information based on DDPM.

9. Pipeline Enhancements Implementation Details

9.1. Label Generator

The visualisation of the conditions obtained based on the layout condition generator is shown in Fig. 7.

We use the following diversity enhancement strategy to get more diverse layout tags.

9.2. Image Filter

This section describes the image filtering process. The CLIP model computes the cosine similarity sim_{clip} between the global text description and the synthetic image. The pre-trained ResNet101 model, trained on bounding box regions from the original dataset, evaluates the classification confidence for each region. The steps are as follows:

The visual experimental results are shown in the Fig. 10

10. Analysis of Data Distribution

The real DIOR data and corresponding synthetic data are visualized using UMAP downscaling. In this visualization,

Algorithm 1 Bounding Box Data Augmentation with Transformations

Require: Original bounding box coordinates $P = \{(x_1, y_1), (x_2, y_2), (x_3, y_3), (x_4, y_4)\}$, image dimensions $(width, height)$, number of variants $num_variants$

Ensure: Augmented coordinates $\{P'\}$

for each variant **do**

 Sample random transformation parameters: scale s , translation (t_x, t_y) , rotation θ , horizontal flip f_h , vertical flip f_v , and stretch factor $stretch$

 Set image center $C = (width/2, height/2)$

 Initialize augmented coordinates $P' = P$

for each point (x_j, y_j) in P **do**

 Apply transformations:

 Scaling: $(x_j, y_j) \leftarrow (x_j - C_x, y_j - C_y) \cdot s + (C_x, C_y)$

 Translation: $(x_j, y_j) \leftarrow (x_j + t_x, y_j + t_y)$

 Rotation: $(x_j, y_j) \leftarrow R(\theta) \cdot (x_j - C_x, y_j - C_y) + (C_x, C_y)$

 Horizontal flip: if f_h , then $x_j \leftarrow width - x_j$

 Vertical flip: if f_v , then $y_j \leftarrow height - y_j$

 Stretch: if horizontal, $x_j \leftarrow (x_j - C_x) \cdot stretch + C_x$; if vertical, $y_j \leftarrow (y_j - C_y) \cdot stretch + C_y$

end for

 Store augmented coordinates P' for this variant

end for

return Augmented coordinates $\{P'\}$

the synthetic training set represents the original labels encountered by the generative model, while the layout labels in the test set are novel to AeroGen. The result shown as in Fig. 9. Given that DIOR is a dataset with clear inter-category relationships, the visualization area effectively re-

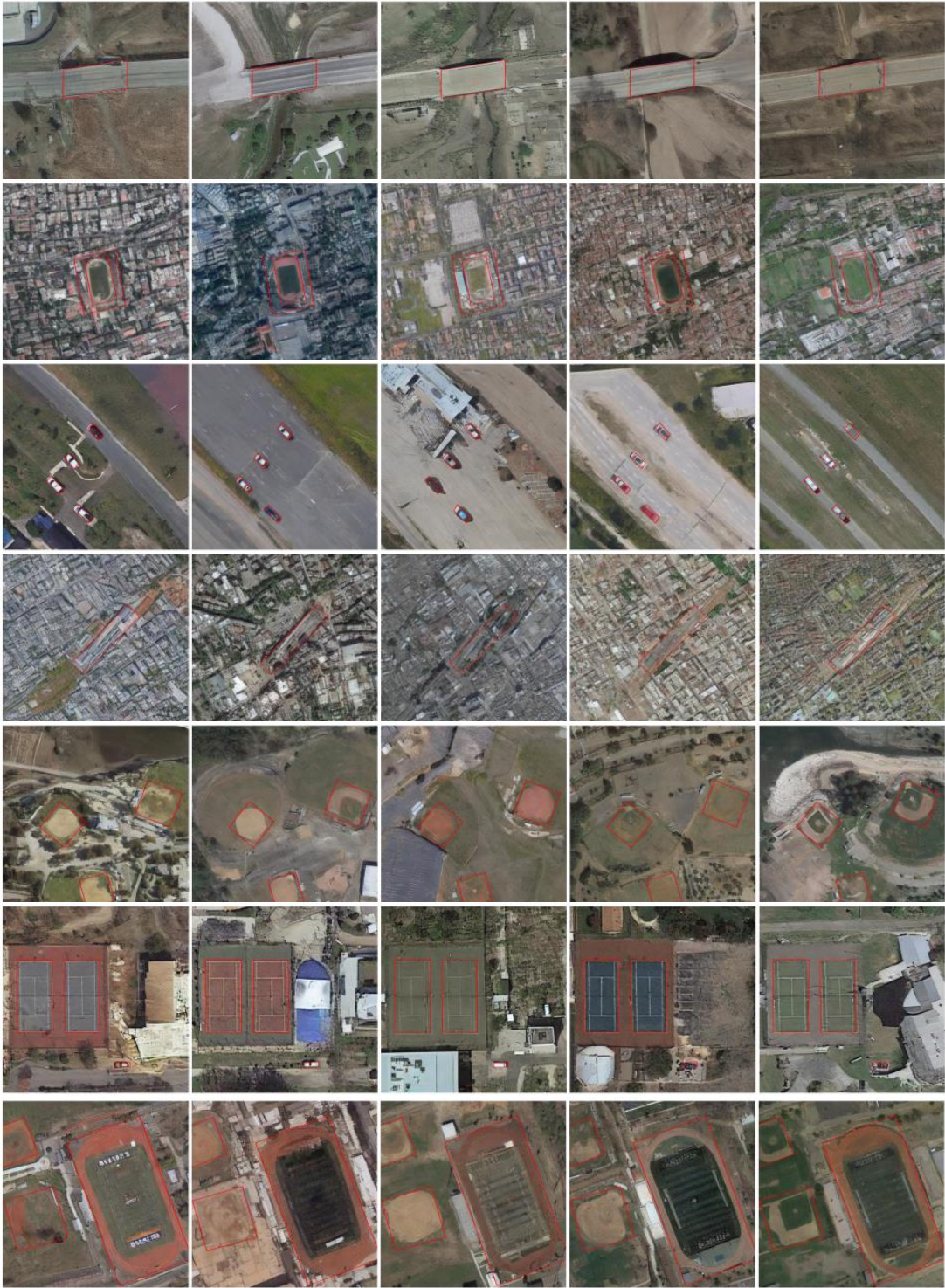


Figure 8. Visualization of AeroGen’s diversity results. Each row of images originates from the same layout and exhibits variations in the corresponding background areas.

flects these relationships. However, the synthetic data does not align perfectly with the real data and appears more con-

centrated under the influence of specific categories.

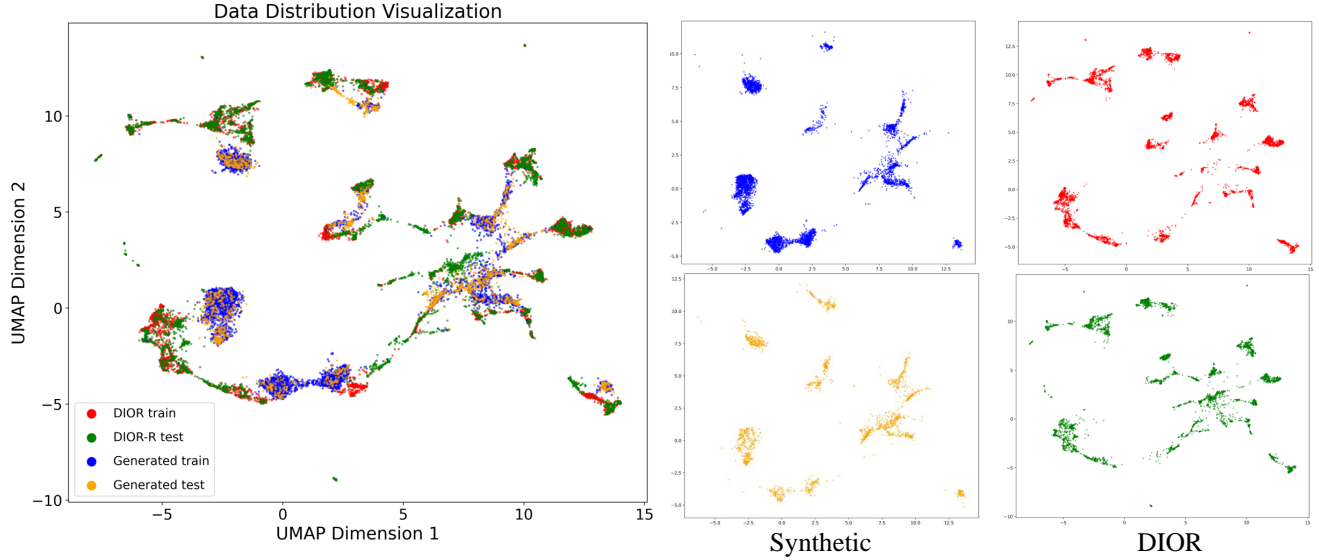


Figure 9. Visualization of data distributions on real-world data and synthetic data.

Algorithm 2 Synthetic Image Processing with Confidence Filtering and CLIP Similarity

Require: Synthetic image I , layout annotations B , global text description T , classifier model M_c , CLIP model M_{clip} , confidence threshold τ

Ensure: Filtered data

```

Compute  $\text{sim}_{clip} = M_{clip}(I, T)$ 
Initialize confidence list  $C = []$ 
Set high-confidence flag  $f_{high} = \text{True}$ 
for each bounding box  $b \in B$  do
    Crop and resize region  $I_b$  from  $I$  based on  $b$ 
    Transform  $I_b$  to tensor and pass through  $M_c$ 
    Compute confidence  $c = \max M_c(I_b)$ 
    Append  $c$  to  $C$ 
    if  $c < \tau$  then
        Set  $f_{high} = \text{False}$  and break
    end if
end for
if  $C \neq \emptyset$  then
    Calculate  $\text{avg}(C)$ ,  $\max(C)$ , and  $\min(C)$ 
end if
if  $f_{high} = \text{True}$  then
    Mark  $I$  as filtered
end if
return Filtered data

```

11. Details of target detection model training

In the target detection experiments, we train and evaluate models for horizontal bounding box (HBB) and rotating bounding box (OBB) detection, respectively. For the HBB

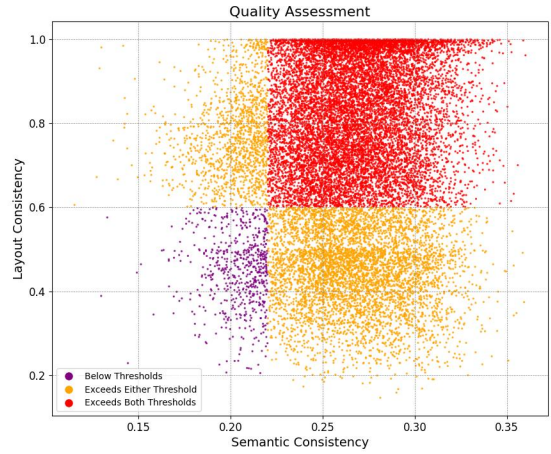


Figure 10. In the image filtering data visualization, the data in the top right corner represents the final filtered synthetic data.

modality, we selected the one single-stage detection model YOLOv8, set an initial learning rate of 0.01, and conducted 50 training epochs to optimize performance on the validation set. Subsequently, the model's performance was evaluated on the test set. For the OBB modality, we utilized Oriented R-CNN for rotating bounding box target detection, employing the official implementation from mmrotate. The optimizer applied stochastic gradient descent (SGD) with a learning rate of 0.0025, momentum set to 0.9, and a weight decay of 0.0001. A segmented learning rate descent strategy (STEP) was employed, featuring 500 warm-up iterations and a warm-up start ratio of 0, followed by 30 training epochs.